Research Square

Preprints are preliminary reports that have not undergone peer review.
They should not be considered conclusive, used to inform clinical practice,
or referenced by the media as validated information.

Investigation of the Structural and Photophysical Properties of Cyclometalated Platinum(II) Complexes as Singlet Oxygen Photosensitizers for Photodynamic Therapy: A DFT Computational Study

Wilaiwan Rosungnoen
Kasetsart University
Wanchai Deeloed
Kasetsart University
Supa Hannongbua
Kasetsart University
Rungtiva P. Poo-arporn
King Mongkut's University of Technology Thonburi
Songwut Suramitr
fsciswsm@ku.ac.th

Kasetsart University

Research Article

Keywords:

Posted Date: May 29th, 2026

DOI: https://doi.org/10.21203/rs.3.rs-8082869/v1

License: This work is licensed under a Creative Commons Attribution 4.0 International License.
Read Full License

Additional Declarations: No competing interests reported.

Investigation of the Structural and Photophysical Properties of Cyclometalated Platinum(II) Complexes as Singlet Oxygen Photosensitizers for Photodynamic Therapy: A DFT Computational Study

Wilaiwan Rosungnoen[1,2], Wanchai Deeloed[1], Supa Hannongbua[1,2],
Rungtiva P. Poo-arporn[3], Songwut Suramitr[1,2]*

[1]*Department of Chemistry, Faculty of Science, Kasetsart University, Bangkok 10900, Thailand.*

[2] *Center for Advanced Studies in Nanotechnology for Chemical, Food, and Agricultural Industries, KU Institute for Advanced Studies, Kasetsart University, Bangkok 10900, Thailand*

[3] *Biological Engineering Program, Faculty of Engineering, King Mongkut's University of Technology Thonburi, Bangkok 10140, Thailand*

Abstract:

The effects of the position of fluorophenyl substituents and the number of fluorine atoms on the structural, electronic, and photophysical properties of cyclometalated Pt(II) complexes (PtM1, PtM2, PtM3, PtP1, PtP2, and PtP3) were investigated computationally using DFT and TD-DFT. Specifically, the frontier molecular orbitals, charge transfer characteristics, absorption and emission spectra, phosphorescence behavior, and oxygen quenching mechanisms of the complexes were examined. All complexes exhibit characteristic MLCT and LLCT transitions. The *meta*-substituted derivatives (PtM1–PtM3) display slightly improved electron transfer characteristics relative to the *para*-substituted analogs (PtP1–PtP3). The emissions exhibit redshifts in the *meta*-substituted complexes, corresponding to a reduced HOMO–LUMO energy gap. Furthermore, all complexes display high triplet exciton generation fractions, indicating efficient intersystem crossing (ISC). The radiative decay rates (k_r) are notably higher for the *meta*-substituted complexes—1.53 x 10^5 s^{-1} (PtM1), 1.68 x 10^5 s^{-1} (PtM2), and 1.72 x 10^5 s^{-1} (PtM3)—compared to the *para*-substituted complexes—1.53 x 10^5 s^{-1} (PtP1), 1.68 x 10^5 s^{-1} (PtP2), and 1.72 x 10^5 s^{-1} (PtP3). Additionally, increasing the number of fluorine atoms further enhances the k_r values, suggesting an improved phosphorescence efficiency. Hence, fluorophenyl-substituted cyclometalated Pt(II) complexes represent promising candidates for photodynamic therapy (PDT). DFT-based theoretical investigations offer a meaningful interpretation of the observed photophysical behavior and

provide design principles for developing new and efficient photosensitizers for PDT applications.

1. Introduction

Oxygen is essential for all living organisms, given its presence in the air, water, blood, cells, and tissues. It plays a critical role in various biological and medical processes, including metabolism [1]. Further, it is involved in the production of adenosine triphosphate (ATP) during oxidative phosphorylation in mitochondria [2] and is required in photodynamic therapy (PDT), a two-stage treatment that utilizes light energy, oxygen, and light-activated compounds (photosensitizers) to induce the destruction of cancerous and precancerous cells through phototoxicity. In PDT, oxygen molecules can be divided into two types: Type I, which generates radicals or radical ions, and Type II, which produces singlet oxygen ($^1O_2$) [3, 4]. Identifying and detecting oxygen levels is strategically essential in many fields, including medical diagnostics [5-11], bioreactors [12, 13], and environmental management [14, 15]. Various detection methods are available; for example, optical methods based on luminescence techniques (fluorescence and phosphorescence) involve quenching with molecular oxygen. Generally, sensors comprise two components—organic and inorganic materials—and are called oxygen-sensitive probes (OSPs). Dynamic quenching occurs via collisions between triplet molecular oxygen and the excited states of OSPs, resulting in reduced emission intensities and shorter excited-state lifetimes. This nondestructive and reversible process enables continuous oxygen monitoring.

Currently, optical oxygen sensors constitute essential tools for real-time oxygen detection, given their distinct advantages over traditional techniques, such as zero oxygen consumption during measurements, complete reversibility, and excellent precision and accuracy [16-19]. Substances commonly used to produce OSPs include complexes of Ir(III) [20], Ru(II) [21], Pd(II) [22], and Pt(II). Among the materials used to create OSPs, cyclometalated platinum(II) complexes are particularly notable for their excellent properties, including long phosphorescent lifetimes and high quantum yields. They typically display planar molecular geometries, which contribute to their highly emissive excited states, and possess other favorable photophysical properties, such as a high color purity and tunable emission energies [22-25].

Cyclometalated complexes are typically built upon tridentate N^C^N or N^N^C ligand frameworks, often accompanied by halogen, pseudo-halogen, or acetylide ancillary ligands. The N^C coordination motif is commonly derived from 2-phenylpyridine (ppy)-type ligands, which are known to produce high-energy phosphorescence. The formation of an anionic metal–carbon bond in N^C-type systems enhances the ligand field strength, elevating the nonemissive metal-centered d–d states and, thereby, minimizing thermal quenching. Furthermore, these ligands can be easily modified with functional groups possessing different electronic and steric properties, allowing for the precise tuning of the photophysical properties of N^C-chelate metal complexes. They generally include bidentate co-ligands, such as acetylacetonate (acac), due to their high triplet energy and excellent solubility [26, 27]. Brooks et al. synthesized a collection of cyclometalated Pt(II) complexes and discovered that several exhibit strong spin–orbit coupling, which enables the mixing of ^{1}MLCT states with ligand-centered $^{3}\pi$-π^* states. This mixing allows for the typically forbidden radiative relaxation of these states to occur efficiently, achieving quantum yields of up to 0.25 at ambient temperatures. In part, halide ions are widely recognized as suitable ligands for stabilizing transition metals. Moving down the halide group, the ionic radius, σ-bond donation capability, trans effect, and bond strength with low-oxidation-state metals progressively increase. Conversely, the π-bond donation ability and bond strength with high-oxidation-state metals decrease from fluorine to iodine [28]. Hu et al. conducted a comparative study on the heavier halogen derivatives, demonstrating a decreasing trend in the emission quantum yield, following the order of F > Cl > Br > I. The complexes containing fluorine exhibit the highest quantum yield of 53.1% [29]. The unique properties of fluorine, including its high electronegativity and relatively small atomic size, make fluoro substituents an ideal choice for tuning the electronic characteristics of a compound. Further, the strong and highly stable C–F bond allows fluorinated groups to stabilize organometallic complexes [30, 31] effectively. Moreover, fluorinated matrices exhibit high oxygen permeability and excellent resistance to irradiation, properties that arise from fluorine's strong electronegativity [32, 33].

These platinum(II) complexes are electrically neutral, air stable, and sublimable, making them highly suitable for applications in optoelectronic devices. Their wide range of excited-state energies and redox potentials further enhances their versatility as tunable photooxidants and photoreductants [34]. Xing's group [35] studied the impact of fluorophenyl substitution in cyclometalated platinum(II) complexes on photostability for oxygen sensing; notably, these complexes are of significant interest for further study. Therefore, our research aims to investigate the photophysical properties of cyclometalated platinum(II) complexes

featuring fluorophenyl ligands at the *meta* and *para* positions and provide theoretical insights that support the development of efficient photosensitizers for PDT.

2. Computational details

All computational results presented herein were obtained using density functional theory (DFT) and time-dependent DFT (TD-DFT), as implemented in Gaussian 16 [36]. The geometries of the ground state (S_0), first singlet excited state (S_1), and first triplet excited state (T_1) of all complexes (shown in Figure 1) were fully optimized via the DFT and TD-DFT methods [37]. The Perdew–Burke–Ernzerhof correlation functional (PBE0) was employed throughout; it was identified as the most appropriate choice based on comparisons with related results [38, 39], considering geometries, photophysical properties, photoelectronic properties, quenching with oxygen, and other parameters. All calculations employed a mixed 6-31G(d,p)/LanL2DZ basis set, where 6-31G(d,p) was used for C, H, N, and O atoms, and LanL2DZ for the Pt(II) atom. Solvent effects of dichloromethane (CH_2Cl_2) were incorporated using the polarizable continuum model (PCM).

To gain deeper insights into the radiative decay process, TD-DFT/PBE0 calculations with spin–orbit coupling (SOC) based on perturbation theory were performed using the Amsterdam Density Functional (ADF 2024.1) [40] at the optimized T_1 geometries. The five lowest scalar relativistic singlet and triplet excitations were included. An all-electron triple-zeta plus polarization basis set was used for Pt, while a double-zeta plus polarization version was applied for all other atoms. The environmental effects of CH_2Cl_2 were taken into account using the conductor-like screening model (COSMO) [41, 42].

The phosphorescence quantum yield is governed by the rates of intersystem crossing (k_{ISC}), radiative decay (k_r), and nonradiative decay (k_{nr}). The intersystem crossing (ISC) rate can be evaluated using Equation 1 [37, 43, 44]:

$$k_{ISC}^{n} = \sum_m \frac{2\pi}{h} \langle S_n | H_{SOC} | T_m \rangle^2 \times FCWD, \quad (1)$$

where $\langle S_n | H_{SOC} | T_m \rangle$ represents the SOC matrix element between the pure spin states S_n and T_m, and FCWD denotes the Franck–Condon weighted density of states, which was evaluated within the framework of Marcus–Leich–Jorter theory, as shown in Equation 2:

$$FCWD = \frac{1}{\sqrt{4\pi\lambda k_B T}} \sum_{n=0}^{\infty} \exp(-S) \frac{S^n}{n!} exp\left[-\frac{(\Delta E + n\hbar\omega + \lambda)^2}{4\lambda k_B T}\right] \quad (2)$$

In this context, λ refers to the Marcus reorganization energy, ΔE is the energy gap between the singlet (S_n) and triplet (T_m) states, $\hbar\omega$ corresponds to the energy of an effective nonclassical vibrational mode involved in the transition, and S is the corresponding Huang–

Rhys factor. The FCWD of structurally related complexes generally lies within a similar order of magnitude [45]. Therefore, the main difference in the FCWD results from the ΔE. In other words, k_{ISC} is primarily governed by the SOC matrix elements and the energy gap between the S_n and T_m states [44].

During the radiative decay process, based on the Born–Oppenheimer approximation and perturbation theory, interactions between the excited triplet state and nearby singlet states can induce SOC. The radiative rate constant (k_r) for the $T_m \rightarrow S_0$ transition can be determined using Equation 3 [46-48]:

$$k_r^{\alpha}(T_m \rightarrow S_0) = \frac{\eta^2}{1.5} E(T_m)^3 \left\{ \sum_n \frac{\langle T_m^{\alpha} | H_{SOC} | S_n \rangle}{E(S_n) - E(T_m)} \right\}^2 \times \frac{f_n}{E(S_n)} \quad (3)$$

Here, η represents the refractive index of the medium, which is set to 1.424 (dichloromethane). $\langle T_m^{\alpha} | H_{SOC} | S_n \rangle$ denotes the SOC matrix element between the m-th triplet excited state (T_m) and the n-th singlet excited state (S_n). The SOC interaction becomes significant when the T_m and S_n states share the same unoccupied orbital distributed over the ligand. In contrast, their occupied orbitals correspond to different Pt *d* orbitals, typically associated with ^{1}MLCT and ^{3}MLCT transitions. f_n is the oscillator strength of the corresponding singlet state, and α refers to the spin sublevel of the triplet state T_m (x, y, or z).

3. Results and discussion

3.1 Geometry of cyclometalated Pt(II) complexes

The present work aimed to predict the photophysical properties of cyclometalated Pt(II) complexes with the preferred substitution of a fluorophenyl group on the 2-phenylpyridine ligand. Figure 1a presents a molecular scheme representing our substitution preferences, at the *para* and *meta* positions of the ligand, and the number of fluorine atoms participating in the substituent. To better describe the charge transfer mechanism, the molecular geometry of the studied complexes in various electronic states (S_0, S_1, and T_1 states) was optimized using DFT calculations. The significant geometrical features in all optimized structures are presented in Table 1. In short, the optimum geometry for all studied complexes involves a square planar complex of a Pt(II) core with a d^8 electron configuration. Typically, the Pt(II) ion is coordinated with two oxygen atoms from the acac ligand, while nitrogen and carbon atoms from the 2-phenylpyridine ligand introduce two further coordinated covalent bonds (Figure 1a). The variation in the geometry upon fluorophenyl substitution was investigated, considering changes in the bond length, bond angle, and dihedral angle, to

construct the square planar Pt(II) complex (see Table 1). No significant differences in molecular geometry arise among the studied complexes in each respective electronic state (S_0, S_1, and T_1).

3.2 Frontier molecular orbital properties

Frontier molecular orbitals play a pivotal role in governing both absorption and emission processes. Photoluminescence properties are determined mainly by the nature of the molecular orbitals (MOs) that dominate the electronic ground state and the lowest excited state. Figure 2 presents key details on the energy levels of the frontier orbitals and the corresponding energy gaps, which are critical parameters for evaluating the luminescent behavior of the complexes.

In this study, the molecular orbital energy levels were modulated by introducing a fluorophenyl group into the cyclometalated Pt(II) complex. The Pt complex with a *meta*-substituted monofluorophenyl group (PtM1) exhibits a HOMO energy level of -5.82 eV, slightly higher than that of the parent Ptppy complex (-5.98 eV). In contrast, the *para*-substituted analog (PtP1) maintains a HOMO energy level of -5.97 eV, comparable to that of Ptppy. Additionally, the PtM1 and PtP1 analogs possess LUMO energy levels of -1.68 and -1.75 eV, respectively, which are lower than the LUMO level of the pristine form (-1.63 eV). Therefore, one can draw a vague conclusion regarding energy gap ($\Delta E_{\mathrm{HOMO–LUMO}}$) engineering through fluorophenyl substitution. The results demonstrate that introducing a fluorophenyl group into the *meta* or *para* positions leads to a slightly deeper LUMO level and an elevated HOMO level, resulting in a narrower energy gap for the substituted Pt(II) complexes. Furthermore, Figure 2a reveals the effect of multiple fluorine atoms on the substituent. Considering samples with similar substituted positions, the addition of a fluoride ion can shift the HOMO and LUMO energy levels of the complexes downward while maintaining the energy gap value. As illustrated in Figure 2a, most *meta*-substituted analogs show an energy band gap of -4.16 eV (PtM1 and PtM2), whereas a value of -4.21 eV is generally observed for *para*-substituted samples (PtP1, PtP2, and PtP3). Among all the modified Pt(II) complexes, the PtM3 complex represents an exceptional case of a large energy gap (-4.20 eV), which is comparable to that of the *para*-substituted samples. Multiplying the fluorine atom causes a downward shift of the band position by approximately 0.8 eV.

The contribution of the frontier orbitals to the Ptppy and modified Pt(II) complexes was studied to describe electron delocalization during the molecular excitation process. The results presented in Figure 2b and Table 2 reveal the frontier orbital contributions in terms of

the molecular constituents. For instance, a composition of 47% π-orbital on the 2-phenylpyridine ligand, 35% d-orbital on the Pt(II) core, and another 18% π-orbital on acac contribute to the ground state (S_0) HOMO of the pristine cyclometalated Pt(II) complex. Meanwhile, introducing the fluorophenyl group to the 2-phenylpyridine ligand induces a change in the HOMO attribute of the modified complexes. For example, the PtM1 sample gains an additional electron from the *para*-substituted fluorophenyl group. In this system, the electron density is predominantly localized on the fluorophenyl ring, contributing approximately 16% of the π-orbital character to the overall complex. In contrast, the *para*-substituted analog (PtP1) exhibits enhanced electron delocalization due to both the additional electron contribution and the extended π-conjugation introduced by the substituent, leading to a more delocalized HOMO across all molecular fragments. Moreover, fluorine substitution on the fluorophenyl ring significantly influences the electronic distribution. As the number of fluorine atoms increases, the HOMO becomes progressively delocalized from the ppy ligand toward the Pt(II) center and the acac ligand. This effect occurs independently of the substitution position.

In addition, the variation in the LUMO attribution was investigated. In most cases, a significant contribution (>80%) of the LUMO is attributed to the 2-phenylpyridine constituent, suggesting its essential role as the chromophore of the cyclometalated Pt(II) complex. The 5d orbital of Pt(II) and the π-orbitals of the acac ligands are associated with a π*-orbital contribution in the LUMO of the ppy ligand. Furthermore, an additional contribution of the LUMO π*-orbital in the fluorophenyl constituent was noted for all *para*-substituted samples (PtP1–PtP3). In these systems, the *para*-substituted fluorophenyl ring extends the π-conjugation, resulting in an increased contribution from the π* orbital. The degree of π* orbital participation correlates with the electron affinity of the fluorophenyl ring, which is determined by the number of fluorine substituents. Increasing the number of fluorine atoms enhances both the electron affinity and π* orbital contribution.

This behavior demonstrates the fine-tuning of the electronic structure, particularly the energy levels and frontier orbital characteristics. It reveals that the energy levels, energy gaps, and orbital nature of the Pt(II) complexes are susceptible to the position of fluorophenyl substitution. Moreover, these observations highlight how different substitution patterns, coupled with extended π-conjugation, modulate the electronic properties of cyclometalated Pt(II) complexes.

3.3 Electronic absorption and emission spectra

To elucidate the electronic transitions of the studied Pt(II) complexes, absorption spectra were calculated using TD-DFT. This study aimed to demonstrate the electronic transitions and delocalization mechanism using optimized models of the complexes in the S_n and T_1 states. Additionally, the interfragment charge transfer was investigated for the complexes using the Multiwfn program, as presented in Table 3.

Table 3 reveals the electronic transitions upon the excitation and emission of the studied Pt complexes. Upon molecular excitation, the S_0-to-S_1 transition occurs. Absorption for all modified complexes based on this transition mode was calculated to appear within the range of 420–434 nm, depending on the energy gap discussed previously. In the case of the modified Pt(II) complexes, the absorption spectra exhibit a redshift with respect to the pristine form upon substitution and an increase in the fluorine number. Regarding the pristine Pt(II) complex, absorption spectra at 411 nm were obtained, with an oscillator strength of 0.0630. In this case, the frontier orbital contribution changes from the HOMO (S_0 state), consisting of contributions from states above, toward the LUMO (S_1 state), in which the LUMO consists of 92% of the π*-orbital in 2-phenylpyridine. In this particular case, frontier orbital migration, which depicts the HOMO–LUMO transition in the pristine Pt(II) complexes, was used as a representative example for all studied complexes (see Figure 3). The contribution of the 5d orbital of Pt(II) and the π-orbital of the acac ligand of the HOMO (S_0 state) migrates toward the π*-orbital of 2-phenylpyridine of the LUMO (S_1 state) upon molecular excitation. Therefore, two important mechanisms, metal-to-ligand charge transfer (MLCT, d(Pt) → π*(ppy)) and ligand-to-ligand charge transfer (LLCT, π(acac) → π*(ppy)), take place as the main processes. These two mechanisms can describe charge migration in the modified Pt(II) complexes, as a high HOMO–LUMO transition (>90%) was also noted.

Apart from excitation, molecular emission can also be explained considering the results in Table 3. In this case, the emission spectra of the considered complexes were determined starting from the optimized geometries of the Pt(II) complexes in the T_1 state, imitating an excited molecule experiencing thermal relaxation before photoemission. Phosphorescence results from the $T_1 \rightarrow S_0$ electronic transition. The emission spectra of all modified Pt complexes show a redshift compared to the case of the pristine form, owing to the presence of an extended π-π conjugated system. The electronic transition from the T_1 to the S_0 state proceeds well in the *para*-substituted complexes due to a significant contribution (approximately 90%) from the LUMO–HOMO transition. The lowest energy emissions of complexes Ptppy–PtP3 occur at 476, 546, 543, 541, 549, 552, and 554 nm, respectively,

corresponding to the experimental emission peaks at 486, 499, 496, 492, 525, 526, and 526 nm, respectively [26]. Overall, the experimental emission wavelengths agree with the calculated results, neglecting the solvent effect during practical work.

3.4 Role of cyclometalated Pt(II) complex in Type II PDT

Type II PDT is a medical treatment that uses a photosensitizer (PS), light, and oxygen to generate singlet oxygen (denoted as $^1O_2$). The PS absorbs light and transfers its energy to molecular oxygen (denoted as $^3O_2$, in the triplet spin state), creating a highly reactive $^1O_2$. This energy transfer mechanism differs from Type I PDT, which relies on electron transfer reactions to generate other reactive oxygen species (ROS).

Figure 3 demonstrates the energy transfer mechanism between a cyclometalated Pt(II) complex and a $^3O_2$ molecule using the Ptppy complex as a representative PS. It is worth mentioning that the singlet-to-triplet ISC of the PS is a key step that occurs on the singlet-state excited PS (^{1}PS*, electronic state = S_1) to generate the triplet-state excited PS (denoted as ^{3}PS*, electronic state = T_n). The ^{3}PS* molecule gradually releases its energy to reach the lowest triplet state (T_1) via thermal relaxation before engaging in a photoemission event ($T_1 \rightarrow S_0$ transition), also called "phosphorescence". Subsequently, the released photon triggers another ISC process in molecular oxygen, generating $^1O_2$, which then damages nearby cellular components and leads to cell death.

Herein, effective photoemission from ^{3}PS* is the key capability of a candidate PS. Firstly, the released photon from the ^{3}PS* must provide sufficient energy for $^3O_2$ ISC. The minimum energy for the oxygen singlet–triplet transition (O_2 $^3\Sigma g^- \rightarrow {}^1\Delta g$ transition) has been experimentally reported as 0.98 eV [7]. Therefore, this value has become a standard qualification for candidate PSs. As shown in Table 3, phosphorescence of the ^{3}Ptppy* complex releases a photon with energy corresponding to the difference between the T_1 and S_0 electronic states. Similarly, the phosphorescence of other studied samples was examined via the $T_1 \rightarrow S_0$ transition. Table 3 presents the energy released from each studied Pt(II) complex. The ^{3}Ptppy* complex emits phosphorescence with a photon energy of 2.60 eV. Meanwhile, the emitted photon energy of the modified Ptppy complexes ranges between 2.24 and 2.29 eV. Hence, the results confirm that all Pt(II) complexes in this study could trigger Type II PDT via a phosphorescence mechanism.

Secondly, the effectiveness of photoemission relies on the quantum yield, which, in turn, determines the rate of $^3O_2$ conversion. In particular, the ISC of PSs, a collection of ^{3}PS* species before photoemission, is a key foundational step and can be predicted computationally

for candidate screening [7, 10]. Herein, significant values associated with an ideal PS candidate, such as the SOC and the ISC energy barrier of $\Delta E(S_1\text{-}T_n)$, were calculated using relativistic quantum chemical methods with the ADF program. Specifically, a low energy barrier and a high SOC strength facilitate effective ISC for a PS. Additionally, the radiative decay rate (k_r), a constant that determines the successful photoemission of a PS, can be estimated. Table 4 presents the calculated ISC energy barriers for the studied Pt(II) complexes, which fall within the narrow range of 0.07–0.10 eV. The Ptppy complex represents the PS with the highest ISC energy barrier (0.10 eV). Meanwhile, fluorophenyl substitution can slightly decrease the energy barrier (by 0.1–0.3 eV; see Table 4). However, the reduction in the energy barrier appears to be independent of the substituted position and the number of fluorine atoms.

The calculated SOC matrix elements, which measure the interaction between an electron's spin and orbital motion, are reported in Table 4. Typically, the stronger the SOC, the more efficient the ISC process and, hence, the higher the probability of phosphorescence and the higher the overall quantum yield of a PS. From the SOC matrix of the Ptppy complex (Table 4), one can deduce that $S_1 \rightarrow T_3$ is a significant transition mode, accompanied by a SOC strength of 348 cm^{-1}. On the other hand, all fluorophenyl-substituted complexes take the $S_1 \rightarrow T_2$ mode as a central transition channel and display a stronger SOC when compared with the unmodified Pt(II) complex (see Table 4). Therefore, fluorophenyl substitution represents a simple and effective modification approach for cyclometalated Pt(II) complexes, as it improves the k_r rate constant of phosphorescence. The *meta* position is the most preferable substitution site for cyclometalated Pt(II) complexes since the SOC strength of the PtM1–PtM3 samples (ca. 900 cm^{-1}) is roughly 1.3-fold higher than that of the PtP1–PtP3 samples (689 cm^{-1}). Furthermore, the multiplication of fluorine atoms is significant for the SOC strength and has a site-dependent habit. As shown in Table 5, multiple fluorine atoms are more beneficial for the *meta*-substituted samples than the *para*-substituted ones. Consequently, the most effective modification was observed in the case of the PtM3 sample, characterized by strong SOC (921 cm^{-1}) and a large k_r constant (1.72×10^5 s^{-1}), which were the optimal values across all samples.

4. Conclusion

In summary, this study examined the effects of fluorophenyl substitution on the structure and photophysical properties of cyclometalated platinum(II) complexes. Optimized geometries revealed that all complexes adopt a square planar structure, with subtle variations in the bond lengths and angles depending on the ligand positions and substitution patterns. Frontier molecular orbital analysis revealed that *meta*-positioned fluorophenyl substituents enhance electron transfer by reducing the HOMO–LUMO energy gap, rendering the complexes superior to *para*-substituted complexes for charge transport. This molecular modification also resulted in a redshift in the UV-Vis absorption spectra of the *meta*-substituted complexes, thereby enhancing their phosphorescence efficiency. Emission spectral analysis further demonstrated that both the substituent position and the presence of fluorine atoms significantly influence the phosphorescence properties, with the *meta*-substituted complexes displaying more pronounced redshifts in their emission peaks. Additionally, an analysis of the ISC rates and decay processes revealed that *meta*-substitution increases both k_{ISC} and k_r, particularly in complexes with a higher number of fluorine atoms, resulting in higher phosphorescence quantum yields and improved photophysical characteristics for oxygen sensing. In conclusion, the complexes favored Type II oxygen quenching, efficiently producing singlet oxygen through energy transfer. Overall, the studied complexes exhibit excellent photophysical characteristics, highlighting their potential as effective PSs for PDT applications.

Acknowledgement

This work was funded by the Faculty of Science, Kasetsart University, under the Graduate Fellowship Program. I sincerely thank my advisor, Assistant Professor Songwut Suramitr, for his invaluable guidance, constructive suggestions, and support in addressing unforeseen challenges. I also acknowledge the Department of Chemistry, Faculty of Science, Kasetsart University, for their continuous assistance and support.

Author's contribution

Wilaiwan Rosungnoen: Investigation, Conceptualization, Methodology, Writing – original draft. Wanchai Deeloed: Writing – review & editing. Supa Hannongbua: Writing – review & editing. Rungtiva P. Poo-arporn: Writing – review & editing. Songwut Suramitr: Supervision, Project administration, Writing – review & editing, Writing – original draft.

Funding

This work was funded by the Faculty of Science, Kasetsart University, under the Graduate Fellowship Program.

Data availability

No datasets were generated or analysed during the current study.

Declarations Conflict of interest

The author declares no competing interests.

References

[1] Dogra V, Kim C (2019) Singlet oxygen metabolism: From genesis to signaling. Front Plant Sci 10:1640.

[2] Semenza G L (2007) Life with oxygen. Science 318(5847):62-64.

[3] Alvarez N, Sevilla A (2024) Current advances in photodynamic therapy (PDT) and the future potential of PDT-combinatorial cancer therapies. Int J Mol Sci 25(2):1023.

[4] Huis In 't Veld RV, Heuts J, Ma S, Cruz LJ, Ossendorp FA, Jager MJ (2023) Current challenges and opportunities of photodynamic therapy against cancer. Pharmaceutics 15(2): 330.

[5] Vatansever F, de Melo WC, Avci P, Vecchio D, Sadasivam M, Gupta A, Chandran R, Karimi M, Parizotto NA, Yin R, Tegos GP, Hamblin MR (2013) Antimicrobial strategies centered around reactive oxygen species-bactericidal antibiotics, photodynamic therapy, and beyond. FEMS Microbiol Rev 37(6):955-89.

[6] Chen S, Ren Q, Zhang K, Sha WEI, Hao T, Xu H, Zhao J, Li Y (2022) A highly sensitive and flexible photonic crystal oxygen sensor. Sens Actuators B Chem 355:131326.

[7] Alberto ME, Mazzone G, Regina C, Russo N, Sicilia E (2020) Theoretical exploration of the photophysical properties of two-component Ru(II)-porphyrin dyes as promising assemblies for a combined antitumor effect. Dalton Trans 49:12653-12661.

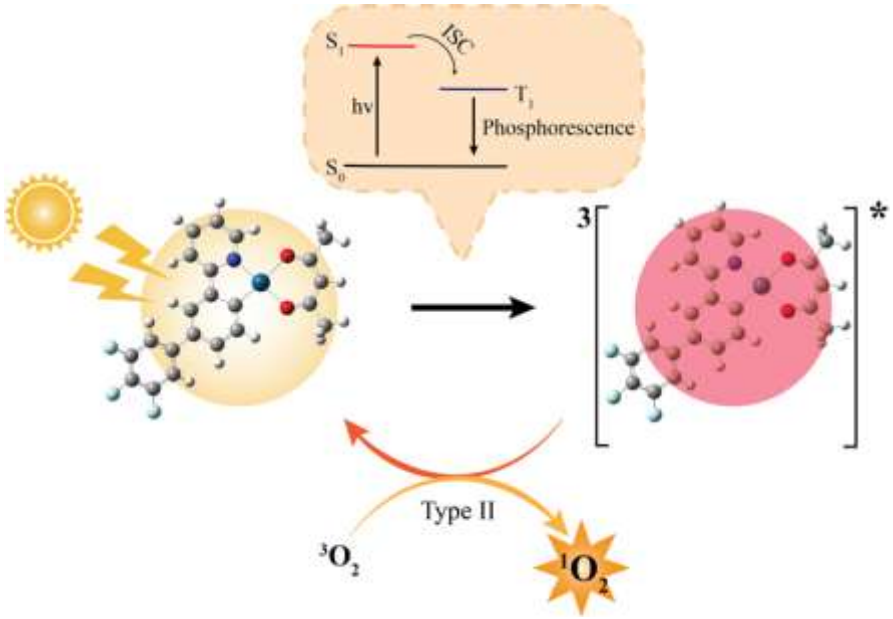
[8] Maharjan PS, Bhattarai HK (2022) Singlet oxygen, photodynamic therapy, and mechanisms of cancer cell death. J Oncol 7211485.

[9] Prejano M, Alberto ME, De Simone BC, Marino T, Toscano M, Russo N (2023) Sulphur- and selenium-for-oxygen replacement as a strategy to obtain dual type I/type II photosensitizers for photodynamic therapy. Molecules 28(7):3153.
[10] Alberto ME, Pirillo J, Russo N, Adamo C (2016) Theoretical exploration of type I/type II dual photoreactivity of promising Ru(II) dyads for PDT approach. Inorg Chem 55(21): 11185-11192.
[11] Zhou CH, Zhao X (2011) Theoretical investigation on quinoline-based platinum (II) complexes as efficient singlet oxygen photosensitizers in photodynamic therapy. J Organomet Chem 696(21):3322-3327.
[12] Renger G, Hanssum B (2009) Oxygen detection in biological systems. Photosynth Res 102(2-3):487-98.
[13] Kim HD, Yi SJ, Kim KC (2013) Simultaneous measurement of dissolved oxygen concentration and velocity field in microfluidics using oxygen-sensitive particles. Microfluidics and Nanofluidics 15(2):139-149.
[14] Alfè M, Gargiulo V, Amati M, Maraloiu VA, Maddalena P, Lettieri S (2021) Mesoporous TiO_2 from metal-organic frameworks for photoluminescence-based optical sensing of oxygen. Catalysts 11(7):795.
[15] Mao Y, Zhao Q, Wu J, Pan T, Zhou B, Tian Y (2017) A highly sensitive and fast-responding oxygen sensor based on POSS-containing hybrid copolymer films. J Mater Chem C 5(44):11395-11402.
[16] Quaranta M, MBorisov S, Klimant I (2012) Indicators for optical oxygen sensors. Bioanal Rev 4(2-4):115-157.
[17] Ning Y, Song X, Zhang H, Liu T, Hao C (2019) The oxygen sensing mechanism of a triphenylamine-based cyclometalated platinum(II) complex. J Lumin 208:46-50.
[18] Xing Y, Liu C, Song X, Li J (2015) Photostable trifluoromethyl-substituted platinum(ii) emitters for continuous monitoring of molecular oxygen. J Mater Chem C 3(10):2166-2174.
[19] Wang XD, Wolfbeis OS (2014) Optical methods for sensing and imaging oxygen: materials, spectroscopies and applications. Chem Soc Rev 43(10):3666-761.
[20] Xing Y, Qiao C, Li X, Li C, Wang H, Li F, Di L, Yang Z (2019) The dependence of oxygen sensitivity on the molecular structures of Ir(iii) complexes and their application for photostable and reversible luminescent oxygen sensing. RSC Adv 9(27):15370-15380.
[21] Plyaka P, Demekhin O, Svetlichnyy D, Zagrebaev A, Budnik A (2021) A fluorescent dissolved oxygen sensor with autocalibration based on ruthenium II tris-bathophenanthroline complex. J Phys Conf Ser 2131:052094.

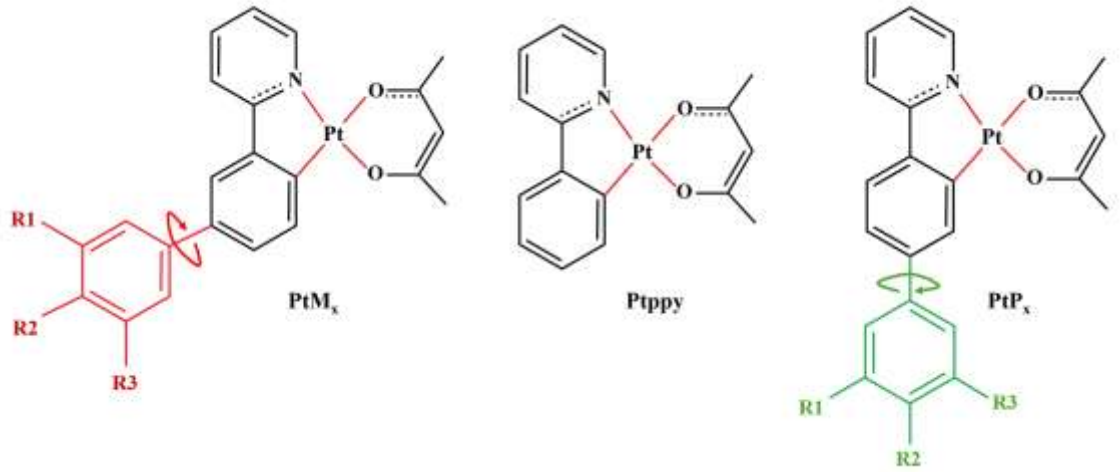
[22] Liu L, Wang X, Hussain F, Zeng C, Wang B, Li Z, Kozin I, Wang S (2019) Multiresponsive tetradentate phosphorescent metal complexes as highly sensitive and robust luminescent oxygen sensors: Pd(II) versus Pt(II) and 1,2,3-triazolyl versus 1,2,4-triazolyl. ACS Appl Mater Interfaces 11(13):12666-12674.
[23] Tong H, Zhao Z, Li G, Gao L, Zhao N, Li P, Jia Y, Zhou C, Zhang M, Wang Y, Hao C, Tang X (2017) TDDFT study on recognition mechanism for the oxygen sensing of the cyclometalated platinum (II) complex. Spectrochim. Acta A Mol Biomol Spectrosc 183: 371-377.
[24] Karakus C, Fischer LH, Schmeding S, Hummel J, Risch N, Schaferling M, Holder E (2012) Oxygen and temperature sensitivity of blue to green to yellow light-emitting Pt(II) complexes. Dalton Trans 41(32):9623-32.
[25] Xing Y, Wang L, Liu C, Jin X (2020) Effects of fluorine and phenyl substituents on oxygen sensitivity and photostability of cyclometalated platinum(II) complexes. Sens Actuators B Chem 304:127378.
[26] Luo Y, Chen Z, Zhang J, Tang Y, Xu Z, Tang D (2016) A cyclometalated (C^C*) platinum(ii) NHC complex decorated via different carboranes to tune the photodeactivation mechanism: a theoretical investigation. RSC Adv 6(114):113513-113521.
[27] Hruzd M, Kahlal S, le Poul N, Wojcik L, Cordier M, Saillard JY, Rodriguez-Lopez J, Robin-le Guen F, Gauthier S, Achelle S (2023) Phosphorescent cyclometalated platinum(II) complexes with phenyldiazine N; C ligands. Dalton Trans 52(7):1927-1938.
[28] Fagnon K, Latens M (2002) Halide effects in transition metal catalysis. Angew Chem Int Ed 41:26-47.
[29] Hu J, Nikravesh M, Shahsavari HR, Babadi Aghakhanpour R, Rheingold AL, Alshami M, Sakamaki Y, Beyzavi H (2020) A C^N Cycloplatinated(II) fluoride complex: Photophysical studies and C(sp(3))-F bond formation. Inorg Chem 59(22):16319-16327.
[30] López O, Crespo M, Font-Bardía M, Solans X (1997) Activation of C-F and C-H bonds by platinum in trifluorinated [C, N, N'] ligands. Organometallics 16:1233-1240.
[31] Crespo M (2011) Fluorine in cyclometalated platinum compounds. Organometallics 31(4):1216-1234.
[32] Amao Y, Miyashita T, Okura I (2000) Optical oxygen sensing based on the luminescence change of metalloporphyrins immobilized in styrene–pentafluorostyrene copolymer film. The Analyst 125(5):871-875.

[33] Amao Y, Miyashita T, Okura I (2001) Platinum tetakis(pentafluoropenyl) porphyrin immobilized in polytrifluoroethylmetacylate film as a photostable optical oxygen detection material. J Fluor Chem 107:101-106.
[34] Brooks J, Babayan Y, Lamansky S, Djurovich PI, Tsyba I, Bau R, Thompson ME (2002) Synthesis and characterization of phosphorescent cyclometalated platinum complexes. Inorg Chem 41:3055-3066.
[35] Xing Y, Liu C, Xiu JH, Li JY (2015) Photostable fluorophenyl-substituted cyclometalated platinum(II) emitters for monitoring of molecular oxygen in real time. Inorg Chem 54(16): 7783-90.
[36] Frisch MJ, Trucks GW, Schlegel HB, Scuseria GE, Robb MA, Cheeseman JR, Scalmani G, Barone V, Petersson GA, Nakatsuji H, Li X, Caricato M, Marenich AV, Bloino J, Janesko BG, Gomperts R, Mennucci B, Hratchian HP, Ortiz JV, Izmaylov AF, Sonnenberg JL, Williams, Ding F, Lipparini F, Egidi F, Goings J, Peng B, Petrone A, Henderson T, Ranasinghe D, Zakrzewski VG, Gao J, Rega N, Zheng G, Liang W, Hada M, Ehara M, Toyota K, Fukuda R, Hasegawa J, Ishida M, Nakajima T, Honda Y, Kitao O, Nakai H, Vreven T, Throssell K, Montgomery Jr. JA, Peralta JE, Ogliaro F, Bearpark MJ, Heyd JJ, Brothers EN, Kudin KN, Staroverov VN, Keith TA, Kobayashi R, Normand J, Raghavachari K, Rendell AP, Burant JC, Iyengar SS, Tomasi J, Cossi M, Millam JM, Klene M, Adamo C, Cammi R, Ochterski JW, Martin RL, Morokuma K, Farkas O, Foresman JB, Fox DJ, Gaussian 16 Rev. C.01. 2016: Wallingford, CT
[37] Huang S, Yang B, Luo S (2020) A theoretical study on spectroscopic properties and quantum yields of chiral-at-metal cyclometalated Pt(II) complexes. J Mol Struct 1199: 126975.
[38] Ernzerhof M, Scuseria GE (1999) Assessment of the Perdew–Burke–Ernzerhof exchange-correlation functional. The Journal of Chemical Physics 110(11):5029-5036.
[39] Adamo C, Barone V (1999) Toward reliable density functional methods without adjustable parameters: The PBE0 model. J Chem Phys 110(13):6158-6170.
[40] Fonseca Guerra C, Snijders JG, te Velde G, Baerends EJ (1998) Towards an order-N DFT method. Theor Chem Acc 99(6):391-403.
[41] Klamt A, Schüürmann G (1993) COSMO: a new approach to dielectric screening in solvents with explicit expressions for the screening energy and its gradient. J Chem Soc Perkin Trans 2 5:799-805.

[42] Li W, Wang J, Yan X, Zhang H, Shen W (2017) Electronic structures and photophysical properties of phosphorescent platinum (II) complexes with tridentate C^N*N cyclometalated ligands. Appl Organomet Chem 32(1):e3929.
[43] Schmidt K, Brovelli S, Coropceanu V, Beljonne D, Cornil J, Bazzini C, Caronna T, Tubino R, Meinardi F, Shuai Z, Bredas JL (2007) Intersystem crossing processes in nonplanar aromatic heterocyclic molecules. J Phys Chem A 111(42):10490-10499.
[44] Marian CM (2011) Spin–orbit coupling and intersystem crossing in molecules. Wiley Interdiscip. Rev Comput Mol Sci 2(2):187-203.
[45] Yu-Tzu Li E, Jiang TY, Chi Y, Chou PT (2014) Semi-quantitative assessment of the intersystem crossing rate: An extension of the El-Sayed rule to the emissive transition metal complexes. Phys Chem Chem Phys 16(47):26184-92.
[46] Zhang ZX, Wei W, Bai FQ, Bibi S, Zhang HX (2017) The phosphorescence properties of a series of diarylethene-containing platinum complexes: the effect of ligand photoisomerization. Org Chem Front 4(11):2191-2201.
[47] Ming Tong GS, Chan KT, Chang X, Che CM (2015) Theoretical studies on the photophysical properties of luminescent pincer gold(III) arylacetylide complexes: the role of pi-conjugation at the C-deprotonated [C; N; C] ligand. Chem Sci 6(5):3026-3037.
[48] Xu Y, Luo Y, Li M, He R, Shen W (2016) Theoretical insights into the photo-deactivation of emitting triplet excited state of (C; N)Pt(O; O) complexes: Radiative and nonradiative decay processes. J Phys Chem A 120(34):6813.

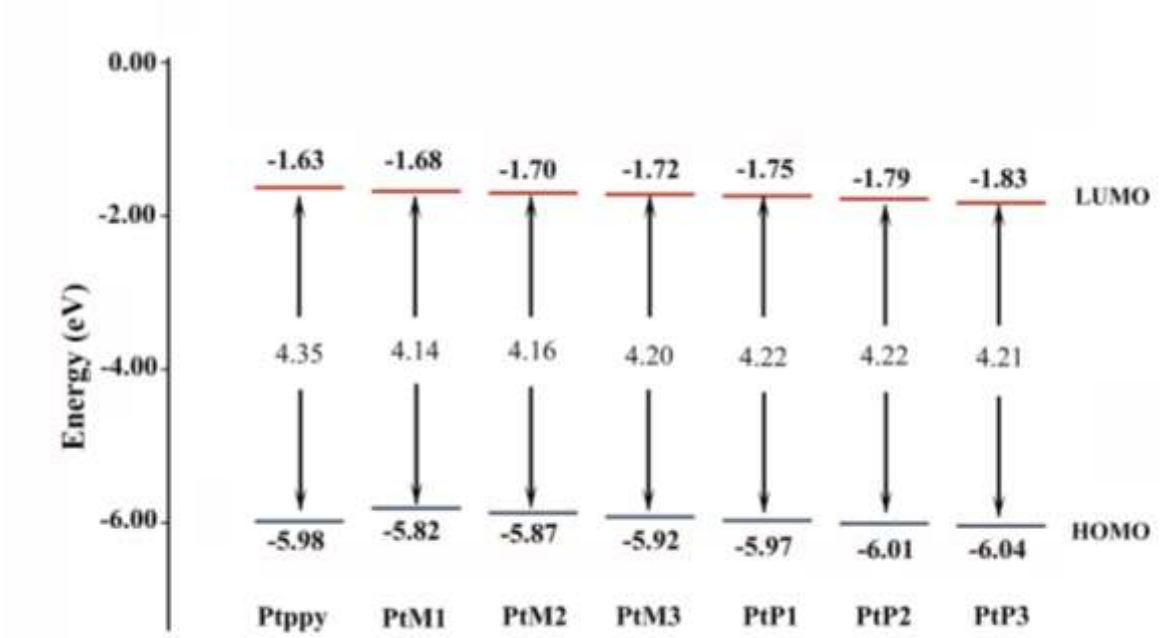


(a)

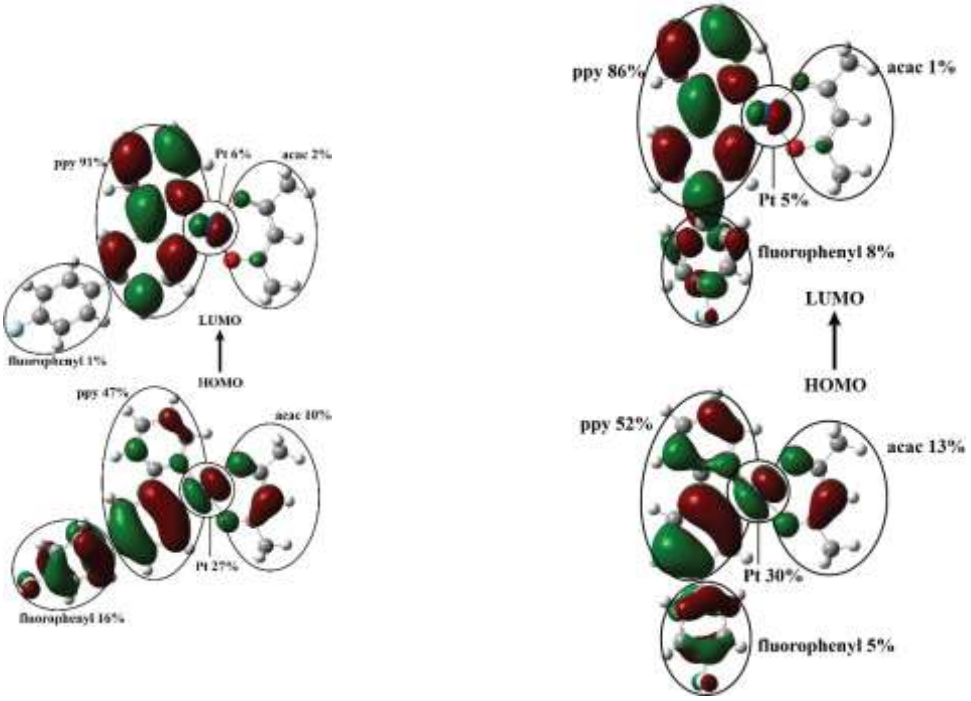


(b)

Figure 1. Chemical structures of investigated cyclometalated Pt(II) complexes with fluorophenyl substituted (x = number of fluoride atoms)



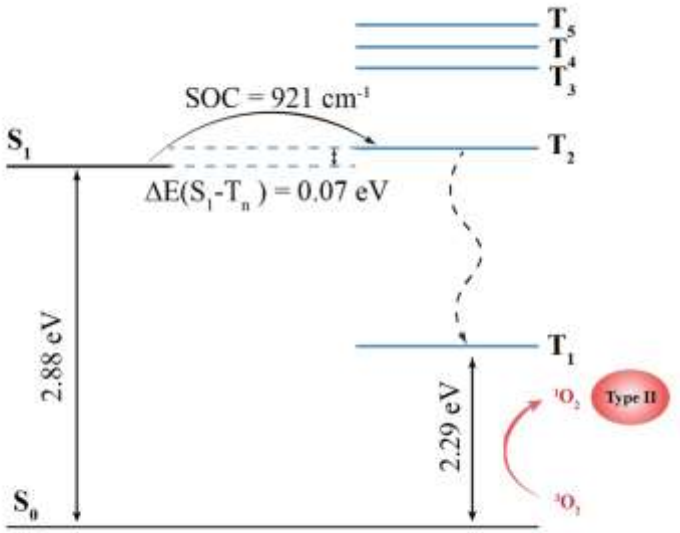
(a)



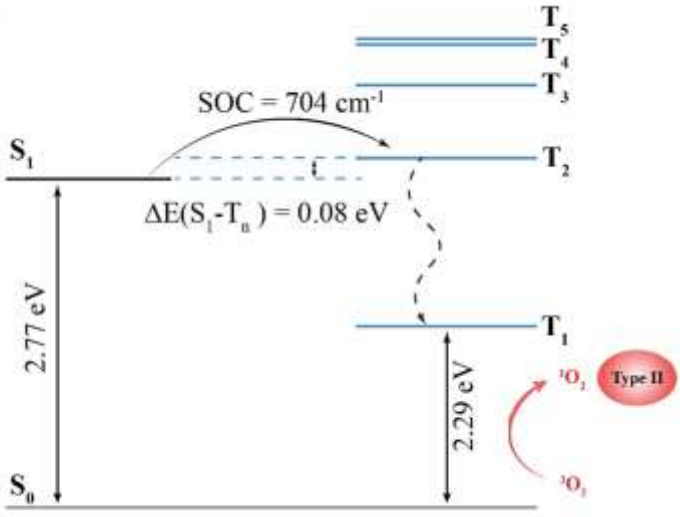
PtM1 PtP1

(b)

Figure 2. (a) The frontier orbitals energy level and ΔE_{L-H} of all Pt(II) complexes. (b) The distribution of electron charge-transfer excitation in singlet excited states of Pt(II) complexes



(a)



(b)

Figure 3. Simplified Jablonski diagram illustrating phosphorescence quenching by O_2 of PtM3 and PtP3 complexes

Table 1. Main optimized geometry parameters of all examined complexes in the ground states, singlet excited, and triplet excited states.

	States	Bond lengths (Å)				Bond angles (degree)		Dihedrals (degree)
		Pt-O_1	Pt-O_2	Pt-N	Pt-C	O_1-Pt-O_2	N-Pt-C	∠(C-C-C-C)
Ptppy	S_0	2.123	2.026	2.052	1.972	91.0	81.4	-
	S_1	2.105	2.060	1.985	1.926	90.6	82.9	-
	T_1	2.120	2.037	1.983	1.952	91.1	82.8	-
PtM1	S_0	2.126	2.024	2.006	1.968	91.1	81.3	143.5
	S_1	2.116	2.057	1.988	1.944	90.5	82.7	152.8
	T_1	2.135	2.036	1.990	1.944	91.0	82.6	150.5
PtM2	S_0	2.125	2.024	2.006	1.967	91.0	81.3	143.9
	S_1	2.113	2.058	1.988	1.924	90.5	82.7	152.2
	T_1	2.132	2.036	1.989	1.945	91.0	82.7	150.0
PtM3	S_0	2.123	2.024	2.006	1.966	91.1	81.3	144.2
	S_1	2.110	2.056	1.988	1.924	90.6	82.7	151.3
	T_1	2.131	2.034	1.988	1.946	91.1	82.7	149.7
PtP1	S_0	2.123	2.024	2.005	1.971	91.1	81.4	144.0
	S_1	2.113	2.052	1.984	1.934	90.8	82.9	153.3
	T_1	2.129	2.030	1.992	1.965	91.1	82.3	168.4
PtP2	S_0	2.122	2.024	1.006	1.971	91.1	81.3	144.4
	S_1	2.112	2.051	1.985	1.933	90.8	82.9	154.6
	T_1	2.127	2.022	1.0993	1.64	91.1	82.3	170.6
PtP3	S_0	2.120	2.024	1.006	1.970	91.2	81.3	144.3
	S_1	2.106	2.052	1.982	1.933	90.9	82.9	154.9
	T_1	2.126	2.029	1.993	1.963	91.2	82.4	171.1

Table 2. Compositions (%) of frontier MOs in the ground state for Pt(II) complexes.

	Orbital	Contribution (%)				Contributions
		Pt	ppy	acac	fluorophenyl	
Ptppy	HOMO	35	47	18	-	π(ppy) + d(Pt) + π(acac)
	LUMO	6	92	2	-	π*(ppy)
PtM1	HOMO	27	47	10	16	π(ppy) + d(Pt) + π(fluorophenyl) + π(acac)
	LUMO	6	91	2	1	π*(ppy)
PtM2	HOMO	29	46	12	13	π(ppy) + d(Pt) + π(fluorophenyl) + π(acac)
	LUMO	6	91	2	1	π*(ppy)
PtM3	HOMO	30	45	14	10	π(ppy) + d(Pt) + π(acac) + π(fluorophenyl)
	LUMO	6	92	1	1	π*(ppy)
PtP1	HOMO	30	52	13	5	π(ppy) + d(Pt) + π(acac)
	LUMO	5	86	1	8	π*(ppy) + π*(fluorophenyl)
PtP2	HOMO	32	49	16	3	π(ppy) + d(Pt) + π(acac)
	LUMO	5	83	1	11	π*(ppy) + π*(fluorophenyl)
PtP3	HOMO	33	46	19	2	π(ppy) + d(Pt) + π(acac)
	LUMO	4	82	1	13	π*(ppy) + π*(fluorophenyl)

Table 3 Electronic transition data from PBE0/6-31G(d,p) for all examined complexes

Complexes	States	E_{Ex} (nm)	E_{Ex} (eV)	Oscillator strength	Configuration	Expt [25] (nm)
Absorption						
Ptppy	$S_0 \rightarrow S_1$	411	3.02	0.0630	HOMO → LUMO (93%)	389
PtM1	$S_0 \rightarrow S_1$	434	2.86	0.0556	HOMO → LUMO (95%)	397
PtM2	$S_0 \rightarrow S_1$	429	2.89	0.0578	HOMO → LUMO (94%)	397
PtM3	$S_0 \rightarrow S_1$	423	2.93	0.0595	HOMO → LUMO (94%)	404
PtP1	$S_0 \rightarrow S_1$	420	2.95	0.1924	HOMO → LUMO (92%)	405
PtP2	$S_0 \rightarrow S_1$	421	2.95	0.1878	HOMO → LUMO (92%)	405
PtP3	$S_0 \rightarrow S_1$	422	2.94	0.1759	HOMO → LUMO (92%)	405
Emission						
Ptppy	$T_1 \rightarrow S_0$	476	2.61	0.0000	HOMO → LUMO (75%)	486
PtM1	$T_1 \rightarrow S_0$	546	2.27	0.0000	HOMO → LUMO (74%)	499
PtM2	$T_1 \rightarrow S_0$	543	2.28	0.0000	HOMO → LUMO (72%)	496
PtM3	$T_1 \rightarrow S_0$	541	2.29	0.0000	HOMO → LUMO (72%)	492
PtP1	$T_1 \rightarrow S_0$	549	2.26	0.0000	HOMO → LUMO (91%)	525
PtP2	$T_1 \rightarrow S_0$	552	2.25	0.0000	HOMO → LUMO (90%)	526
PtP3	$T_1 \rightarrow S_0$	554	2.24	0.0000	HOMO → LUMO (89%)	526

Table 4. The SOC matrix elements, the singlet-triplet energy gaps (ΔE) of primary ISC channels, and the radiative decay rate (k_r).

Complexes	(S_1, T_n)	Excitation	SOC (cm^{-1})	$\Delta E(S_1\text{-}T_n)$ (eV)	k_r ($x10^5$) (s^{-1})
Ptppy	(1, 3)	S_1: H → L (93%),	-	-	-
		T_3: H-1 → L+1 (61%)	348	0.10	0.28
PtM1	(1, 2)	S_1: H → L (95%),	-	-	-
		T_2: H-1 → L (49%)	881	0.10	1.53
PtM2	(1, 2)	S_1: H → L (94%),	-	-	-
		T_2: H-1 → L (49%)	900	0.08	1.68
PtM3	(1, 2)	S_1: H → L (94%),	-	-	-
		T_2: H-1 → L (50%)	921	0.07	1.72
PtP1	(1, 2)	S_1: H → L (92%),	-	-	-
		T_2: H-1 → L (67%)	699	0.08	1.22
PtP2	(1, 2)	S_1: H → L (92%),	-	-	-
		T_2: H-1 → L (65%)	664	0.07	1.23
PtP3	(1, 2)	S_1: H → L (92%),	-	-	-
		T_2: H-1 → L (63%)	704	0.08	1.23

Supplementary Files

This is a list of supplementary files associated with this preprint. Click to download.

- 05ElectronicSupplementaryInformation.docx